An-Najah University Journal for Research – A
Natural Sciences

Downscaling of Thermal Images Over the Gaza Strip Using the Land Surface Temperature—Spectral Indices Relation: Case Study; Hot, Arid, and Semi-Arid Areas

Received: 19/11/2022, Accepted: 22/2/2023, DOI: 10.35552/anujr.a.37.2.2103

Wiesam Essa[1,*] & Rachid Lhissou[2]

Abstract: Many thermal sharpening applications are evaluated in temperate and subtropical climate regions, which are commonly characterized by the presence of the urban heat island (UHI) phenomenon. However, similar studies are rarely found in hot, arid, and semi-arid climate cities, where an urban cool island (UCI) phenomenon exists. Recent research shows that the spectral characteristics of land covers and their responses to LST are different based on their climatic type. Resultantly, spectral indices (SIs) show different evaluations to be successfully used in sharpening techniques like the DisTrad, to sharpen LST over several land covers, especially in urban areas. The main objectives of this study are; 1)- to evaluate the spatial relationship between LST and a number of most commonly used urban's remote sensing SIs (21 SIs described in table 2) over the Gaza Strip in two land cover scenarios: all land covers "All" and the urban mask "urban"; 2)- to downscale aggregated low-resolution Landsat 8\LST image at 1000 m to a higher resolution of 100 m. Spectral indices and land surface temperature are calculated using the Landsat 8 image of summer 2017. Spatial regression analysis between SIs and LST within the "All" land cover class and at 1000 m resolutions show the best SIs that have the highest correlation (R^2) with LST are DBSI (0.66) and ABEI (0.59). While in the "urban" class, the same indices shows also the highest correlation; BAEI (0.57) and DBSI (0.64). Moreover, statistical validation with LST observation at 100m resolution (Landsat 8\LST), DisTrad was found successful to downscale LST to 100 m resolution over UCI areas using the indices ABEI and DBSI with the highest correlation (R^2) over the "All" class (0.77 and 0.73 respectively) and over the "urban" mask using DBSI (0.59) and BAEI (0.58)..

Keywords: DisTrad, Landsat 8, urban cool island (UCI), thermal sharpening, spectral indices (SIs), land surface temperature (LST).

Introduction

Several studies show the usefulness of land surface temperature (LST) in characterizing and monitoring the urban heat island (UHI) (Essa et al., 2013, 2012). UHI phenomenon is typically found in temperate climate zones, where cities are warmer than their surroundings (Voogt and Oke, 2003). Hundreds of UHI studies worldwide have been investigated in temperate and subtropical climate areas (Sun and Pinker, 2003; Nichol, 1996), which helps produce many established techniques such as thermal downscaling. Thermal downscaling of low-resolution satellite imagery to higher spatial and temporal resolutions was essential for enriching the UHI studies. However, in the last few years, several studies (Essa and Lhissou, 2021; Yang et al., 2017; Rasul et al., 2017; Haashemi et al., 2016; Rasul et al., 2016; Theeuwes et al., 2015; Rasul et al., 2015) have reported the inversion of the UHI phenomenon, called the cool urban island (UCI). In UCI areas, the cities in hot climates (desert, arid and semi-arid) become cooler than their periphery. City peripheries are typically covered with natural land covers such as bare soil and sand found to play an essential role in reversing the urban cool island (UCI) phenomenon (Essa and Lhissou, 2021). The dry bare soil and sand emit higher LST within the urban surroundings than in the urbanized area (Rasul et al., 2015). Essa et al. (2021) review the UCI effect over different cities in dry or semi-arid regions with dry surroundings such as Dubai, Abu Dhabi, Beijing, Okayama, Chang-Zhu-Tan, Tehran, Isfahan, and Kuwait. Research on UCI is still in the preliminary stage, where in-depth research on quantifying and modeling the thermal environment of arid and semi-arid is in slow progress (Rasul et al. 2015, 2017., Li et al., 2011).

Various spaceborne thermal sensors provide a free source of land cover information critical for advancing urban studies, scanning all world cities of different climate zones. However, for technical constraints (Table 1), only high spatial or high temporal resolution LST data are available from those sensors, sensors (Essa et al., 2013). The LST pattern at a 100 m scale is considered adequate for monitoring the complex intra-urban variations of LST (Essa et al., 2017; Nichol, 1996). Because of that, thermal downscaling to such a scale became fundamental, cost-effective, and available to provide LST data with higher spatial and temporal data at once.

1 Department of Geography, Faculty of arts and humanities, Al-Aqsa University, Gaza, Palestine.
*Corresponding author: wiesam@alaqsa.edu.ps
2 Institut National de la Recherche Scientifique, Centre ETE, Québec, Canada.

Table (1): Technical characteristics of operational thermal satellite sensors.

Sensor-Platform	Reference	Spatial Resolution (m)	Spectral-Resolution (µm)	Temporal-Resolution (day/minute/hour)
INSAT 3A[1]	(INSAT 3A. 2020)	8000	VHRR/2 band: 10.5 - 12.5	23 min
GEOS imager[2]	(Essa et al., 2017)	5000	Band 4: 10.2–11.2 Band 5: 11.5–12.5	3 h
Meteosat 8- MSG serviri[3]	(Bechtel et al., 2012)	3300	TIR Band: 10.8 - 12	15 min
AVHRR–NOAA[4]	(Tucker at al., 1996)	1100	Band 4: 10.3–11.3, Band 5: 11.5–12.5	0.5 d
MODIS–Terra	(Zhou et al., 2014)	1000	Band 31 - 36: 10.78–14.39	1 to 2 d
AATSAR[5]–Envisat	(Soria and Sobrino. 2007)	1000	Band 11, Band 12	35 d
Sentinel-3A	(Coppo et al., 2015)	1000	Bands S7-S9: 3.74–12.00 Level-2 LST product	27 d
TM–Landsat 5	(Sobrino et al., 2004)	120	Band 6: 10.4–12.5	16 d
OLI & TIRS[6]–Landsat8	(Tan et al., 2016)	100	Band 10: 10.60–11.19 Band 11: 11.50–12.51	16 d
ASTER[7]–Terra	(Wang and Liang. 2009)	90	Band 10 to band14: 8.125–11.65	16 d
Landsat 7 - ETM+	(Rahman et al., 2017)	60	Band 6: 10.4–12.5	16 d

1: “Indian National SATellite Very High-Resolution Radiometer”.
2: “Geostationary Operational Environmental Satellites”.
3: “Meteosat Second Generation Spinning Enhanced Visible and Infrared Imager”
4: “Advanced Very High-Resolution Radiometer-National Oceanic and Atmospheric Administration”
5: “Advanced Along-Track Scanning Radiometer”
6: “Operational Land Imager and Thermal Infrared Sensor”
7: “Advanced Spaceborne Thermal Emission and Reflection Radiometer”

Many researchers (Rasul et al., 2016; Essa et al., 2013, 2012; Stathopoulou and Cartalis. 2009; Agam et al., 2007a, 2007b; Kustas et al., 2003) reviewed the remote sensing thermal downscaling methods and grouped them into physical and statistical methods, namely depends on the type of relationship that exists between LST and ancillary data used in downscaling. The statistical models for downscaling LST are more valuable than physical models for their easy implementation and acceptable accuracy (Yang et al., 2017; Essa et al., 2013, 2012). Downscaling methods are cost-efficient for producing sharpened images similar to high-resolution satellite imagery (Essa et al., 2017). Moreover, statistical downscaling models show strong potential and applicability because the same remote sensors allow the generation of many co-registered land surface information throughout the spectral and thermal bands. Various statistical downscaling techniques have been developed, during the last 10 years for downscaling UHI\LST over urban areas including: “the disaggregation procedure for radiometric surface temperature – DisTrad” (Eswar et al., 2016; Essa et al., 2013, 2012; Kustas and Norman, 2003), “A nonlinear method of DisTrad – NL-DisTrad” (Bindhu et al., 2013), “improved DisTrad with residual error parameterization” (Essa et al., 2017), “temperature sharpening – TsHARP” (Agam et all., 2007a, 2007b, 2008), “pixel block intensity modulation – PBIM” (Stathopoulou and Cartalis, 2009), “high-resolution urban thermal sharpener – HUTS” (Dominguez et al., 2011), “area-to-point regression kriging – ATPRK” (Granero-Belinchon et al., 2019), “adaptive area-to-point regression kriging – AATPRK” (Granero-Belinchon et al., 2019), “multiple linear regressions – MLR” (Wicki and Parlow, 2017), “high-resolution land cover-based emissivity data” (Agathangelidis & Cartalis, 2019), “a method that first performed principal component analysis over their predictors and then applied linear regression to the principal components” (Zaksek and Ostir, 2012), “a method that used support vector machine regression to determine the relationship between LST and predictors” (Zhou et al., 2011), “a method that proposed annual cycle parameters (ACP) from multi-temporal LST data as downscaling predictors” (Agathangelidis & Cartalis, 2019; Bechtel et al., 2012; Bechtel, 2012), “multiple predictor variables” (Zaksek and Ostir, 2012), and “the adjusted stratified stepwise regression method – Stepwise” (Zhu et al., 2012). Although the potential utility of those techniques has been tested for downscaling LST over UHI areas, their evaluation over UCI areas is not nonexistent. DisTrad (Kustas et al., 2003) is the most used method (Bala et al., 2019). It is gaining attention due to its “simplicity, physical basis, and operational capability” (Bala et al., 2019; Essa et al., 2017; Eswar et al., 2016). Also, DisTrad is the basic form for several other downscaling methods such as the TsHARP, HUTS, the NL-DisTrad, and the improved DisTrad. DisTrad successfully adapted to downscale UHI\LST in urban areas based on the functional relationship between LST and different SIs indicators of different land covers (Essa et al., 2013, 2012; Sun and Pinker, 2003). The DisTrad framework considers the functional relationship between the high-resolution land covers (e.g., SIs) and the low-resolution LST as an input for the sharpening procedure. The original DisTrad technique was developed for agricultural areas, based on the LST- Normalized Difference Vegetation Index (NDVI) relationship (Kustas et al., 2003), especially in temperate and subtropical climate regions, where vegetation cover is dominant. NDVI index (Granero-Belinchon et al. 2019), the vegetation fraction index (Wicki and Parlow. 2017), and the impervious percentage index (Essa et al., 2012) are successfully integrated into DisTrad to sharpen LST in agricultural and urban areas of temperate climate areas. However, the behavior of the LST pattern differs from different land covers (Bala et al., 2019) and climate zones. Until now, very little research has evaluated the utility of spectral indices (SIs) over UCI areas of hot, arid, and semi-arid areas for thermal sharpening purposes.

The SIs-LST functional relationship is the fundamental base for the statistical sharpening methods, especially when it is a typical scale-independent relationship, then, a course LST image can be utilized at the higher resolution of the SIs. The successful implementation of downscaling methods over complex land cover surfaces is still limited by the selection of an appropriate environmental predictor, which is considered an important task (Govil et al., 2019; Bechtel et al., 2012). Regardless of the exact statistical downscaling method used, the accuracy of thermal downscaling relies on the robustness of the LST - sharpening predictors relationship (Feng et al., 2020). Spectral indices are commonly used as a robust LST sharpening predictor in different

land-cover types, which possess a robust representation of the land cover and a high correlation with LST for successful downscaling LST procedures. For example, Essa et al. (2012) investigated 16 different SIs and found that the impervious percentage index has the best correlation with LST in urban areas. Pan et al. (2018) indicated that "the normalized difference sand index (NDSI)" has the best correlation with LST in an arid oasis-desert ecotone of Zhangye City, NDSI - LST higher correlation in the humid region (Nanjing City) but is less accurate in the arid region. However, the LST-NDVI relationship was found weak to sharpen LST in urban areas (Essa et al., 2013, 2012; Zaksek and Ostir, 2012; Stathopoulou and Cartalis, 2009). Moreover, integrating several SIs does not mean better downscaling; however, finding a good index combination to improve the downscaling performance should be addressed in future research (Granero-Belinchon et al., 2019). The functional relationship between SIs and UCI\LST could also depend on the season and climatological parameters as well as the city's urban structure and urban material differences, land cover type, and its biophysical bio-thermal properties (Essa et al., 2021). Resultantly, the robustness of such a relationship in heterogeneous urban areas of hot arid, and semi-arid climate areas is a critical issue for much upcoming research.

In this study, DisTrad was selected for the LST sharpening procedure. Moreover, the study evaluates the sharpening procedure of an image at 1000 m resolution comparable with the daily MODIS\LST product to target 100 m resolution (like Landsat8\LST). The land cover classification map used in this application was calculated from the same Landsat 8 images for the best-case scenario, this means that SIs and LST pixels are perfectly geographically co-registered. Consequently, no error sources for SIs - LST statistical relationship. Hence, the aims of this study are;

1. To evaluate the statistical relationship between a sum of frequently used spectral indices (21 indices) and LSTs over the hot arid, and semi-arid climate area of the Gaza Strip. The full description of these SIs is mentioned in table 2.

2. To evaluate the DisTrad method to downscale simulating MODIS\LST image (1000 m) using two land cover scenarios; the “All” classes scenario (urban, vegetation, bare soil, and sandy soil), and the urban mask “urban”.

Data and Methods

Study Area

The Gaza Strip is bounded by longitudes 616140 and 648576 East and latitudes 3455040 and 3496078 North, with an approximate area of 365 km^2. It is one of the greatest densities of the population around the world (≈ 5770 p/km^2) (Essa and Lhissou, 2021). Gaza Strip is bordered by the Mediterranean Sea from the East, with 40 km along the East. Moreover, Gaza Strip is surrounded by the Sinai desert from the South and the Negev desert from the East. Rainfall estimation is decreasing from the north (400 mm) to the south (200 mm), where most of the rainfall occurs from October to March, the rest of the year being dry (PHG, 2002). The main soil types in the Gaza Strip originate from the dune sands and loess soils (Dudeen, 2001). The Gaza Strip has a semi-arid climate, temperate winter, and hot summer. Gaza Strip represents a transition area between a temperate Mediterranean climate (West to North) and an arid desert climate (East to South) (Adnan et al., 2010). The land-covers map (LC) of the Gaza Strip is available from Essa and Lhissou (2021). LC map (Figure. 2) shows the high variability of the urban landscape pattern and its heterogeneity covers an area of about ~43.5 km^2, with higher densities occurring in the urban core and lower densities in the periphery with bushes and trees. The wide range of LST values and varieties in LC classes within the Gaza Strip makes the area an adequate case for thermal downscaling application over the Gaza Strip.

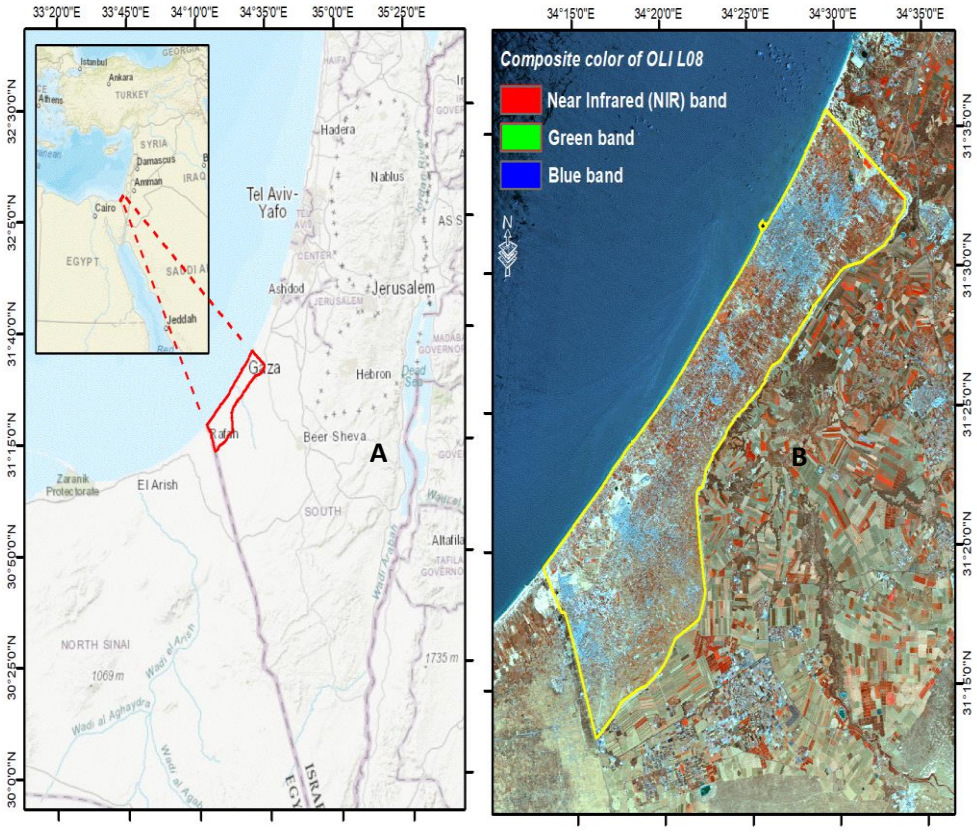

Figure (1): Study area of the “Gaza Strip” indicating the regional (A) and the local location (B) using composite color of L08\OLI.

Landsat 8 Derived Data

A Landsat 8 image used in this application was acquired on June 16, 2017 (05.50 pm). The L8\multispectral bands (operational land imager-OLI) and L8\LST (band 10) images capture data at 30 m and 100 m respectively. However, both the multispectral and thermal bands are geo-registered and delivered with a 30 m spatial resolution. The Landsat 8 data were atmospherically corrected using FLAASH model.

The method for retrieving the LST was carried out using the "Semi-Automatic Classification Plugin (SCP)" (Congedo et al., 2016), which allows the use of the "free-open-source software QGIS" as remote sensing software. With this plugin, temperatures are retrieved automatically from the metadata of the image acquired by the Landsat-8 satellite sensor. Mallick et al. (2012) provide the emissivity (e) values of various land cover types.

The multispectral bands of Landsat 8 (L8\OLI) image used for calculating 21 SIs are mentioned in Table. 2 (adapted from Essa, W. (2022)). The SIs that integrate LST data are not used in this application because it is not scientifically correct in drawing a correlation between LST images and indices that have the same LST data. It is also supposed that thermal data are not present. Because of that, only the spectral band's-based indices are considered for this application to be evaluated. The SIs indicated in previous studies are based on their use to map; urban, vegetation, and bare soil land covers. L8/LST and SIs were aggregated through the spatial averaging to images to 100 m and 1000 m resolution. The functional relationships between those SIs and LST were found in the literature to be a useful basis for LST sharpening methods (Essa et al., 2013, 2012; Agam et al., 2007a; Kustas et al., 2003).

Table (2): 21 remote sensing spectral indices (SIs) used for statistical correlation with the Landsat 8\land surface temperature (LST) including symbol, name, description, and reference (adapted from Essa, W. (2022)).

Index ID	Index Name	Description
ABEI	"Automated Built-Up Extraction Index"	$0.312\,\rho Costal + 0.513\,\rho Blue - 0.086\,\rho Green - 0.441\,\rho Red + 0.052\,\rho NIR - 0.198\,\rho SWIR1 + 0.278\,\rho SWIR$
BAEI	"Built-up Area Extraction Index"	$\frac{\rho RED + 0.3}{\rho Green + \rho SWIR1}$
BI	"Bare Soil Index"	$BI = \rho RED + \rho SWIR1 - \rho NIR$
BRBA	"Band Ratio for Built-Up Area"	$\frac{\rho RED}{\rho SWIR1}$
BSI	"Bare Soil Index"	$\frac{(\rho SWIR1 + \rho RED) - (\rho NIR + \rho BLUE)}{(\rho SWIR1 + \rho RED) + (\rho NIR + \rho BLUE)}$
BUI	"Built-Up Index"	$NDBI - NDVI$
DBSI	"Dry Bare-Soil Index"	$\frac{\rho SWIR1 - \rho Green}{\rho SWIR1 + \rho Green}$ - NDVI
ENBI	"Enhancement Built-Up Index"	$NDWI - FVC$
IBI	"Index-Based Built-Up Index "	$\frac{(NDBI - (SAVI + MNDWI))/2}{(NDBI + (SAVI + MNDWI))/2}$
P_Imp	"Impervious Fraction"	$P\_imp = 1 - P_v$ $P_v = \frac{(NDVI) - (NDVI)_s}{(NDVI)_s + (NDVI)_s}$
MSAVI2	"Modified Soil-Adjusted Vegetation Index"	$\frac{2 \times \rho NIR + 1 - \sqrt{(2 \times \rho NIR + 1)^2 - 8(\rho NIR - \rho RED)}}{2}$
NBI	"New Built-Up Index"	$\frac{\rho RED\ x\ \rho SWIR1}{\rho NIR}$
NBUI	"New Built-Up Index"	$EBBI - SAVI - MNDWI$
NDBI	"Normalized Difference Built-Up Index"	$\frac{\rho SWIR - \rho NIR}{\rho SWIR + \rho NIR}$
NDSI	"Normalized Difference Soil Index"	$\frac{\rho NIR - \rho RED}{\rho NIR + \rho RED}$
NDVI	"Normalized Difference Vegetation Index"	$\frac{\rho NIR - \rho RED}{\rho NIR + \rho RED}$
SAVI	"Soil Adjusted VI"	$\frac{(\rho NIR - \rho RED)}{(\rho NIR + \rho RED + 1)} \times 1$
UI	"Urban Index"	$\frac{[\rho SWIR2 - \rho NIR]}{[\rho SWIR2 - \rho NIR]}$
VgNIR-BI	"Visible Based Indices"	$\frac{\rho Green - \rho NIR}{\rho Green + \rho NIR}$
VIBI	"Vegetation Index Built-Up Index"	$\frac{\left(\frac{\rho NIR - \rho RED}{\rho NIR + \rho RED}\right)}{\left(\frac{\rho NIR - \rho RED}{\rho NIR + \rho RED}\right) + \left(\frac{\rho SWIR1 - \rho NIR}{\rho SWIR1 + \rho NIR}\right)}$
VrNIR-BI	"Visible Based Indices"	$\frac{\rho RED - \rho NIR}{\rho RED + \rho NIR}$

The land cover map of the Gaza Strip (Figure. 2) was derived from the same L8\OLI image bands to eight land covers using the support vector machine (SVM) method. The land covers include built-up, sand dunes, bare soil, crops, trees, shrubs, greenhouses, and wastewater. The SVM is a supervised classification method based on an artificial neural network analysis developed by Kohonen. (2001). "The advantage of using the SVM method approach is that mixed pixels, which occur in medium-resolution satellite data of urban areas, can be more easily identified and assigned to a separate class". (Kohonen. 2001). This is necessary to resolve the mixed-pixels problem such as bare soil with impervious surfaces. In this study, we used "a non-linear SVM classification with the kernel of the radial base function (RBF), which is widely used and outperforms the other kernels (linear, polynomial, or Gaussian) in several applications including land use and land cover" (DeWitt et al., 2017; Mugiraneza et al., 2019; Ngo et al., 2020). The SVM penalty parameter selected value is high and equal to 100 to increase the cost of misclassifying pixels, while the inverse of the number of bands is used for the gamma term in the RBF kernel. The SVM classifier was trained and validated (with an overall accuracy of 92.50% and kappa coefficient of 0.89) by in-field GPS class samples, whose polygons were verified on the very high spatial resolution Google Earth imagery of the same period of the OLI image. Later, the land cover classes were grouped into two land cover scenarios for this study: 1) the urban mask “urban” and the “ALL” class (all classes without the wastewater).

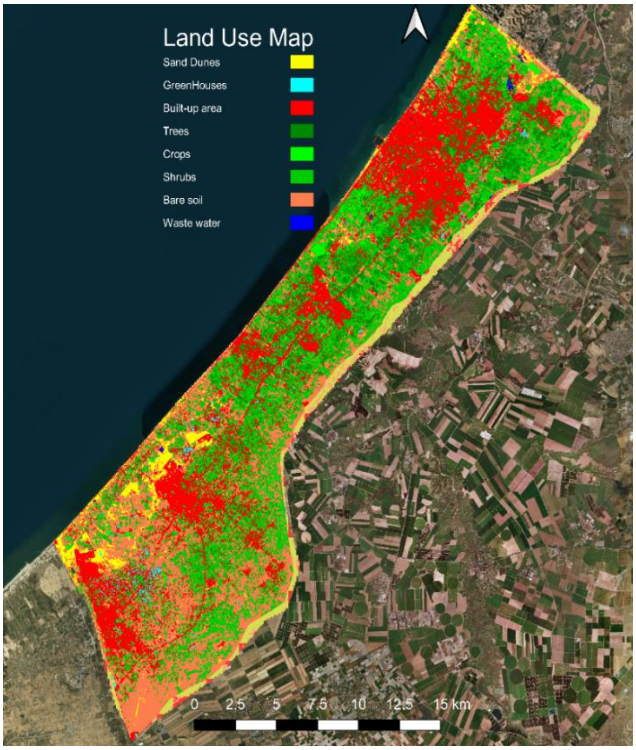

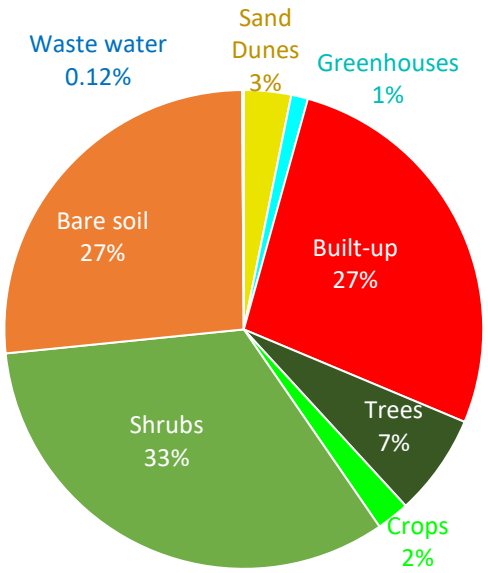

Figure (2): Land-use/Land-cover classification map of the Gaza Strip (June 2017) indicating eight land covers, using the support vector machine (SVM) method (adapted from Essa and Lhissou, 2021).

DisTrad downscaling method.

The first DisTrad sharpening method was developed by Kustas et al. (2003) to estimate LST in vegetated areas using NDVI. SIs are derived from the multispectral high resolutions bands to estimate a higher resolution of LST patterns like SIs resolutions. However, DisTrad was adapted to estimate LST in different land covers like the urban areas (Essa et al., 2017, 2013, 2012). The regression function between SIs and LST at the lower resolution is used as an estimator of LST at the higher resolutions of SIs. "It is assumed that the regression equation is resolution-independent" (Essa et al., 2013, 2012; Kustas et al., 2003). SIs information, 100 m resolution in this application, is used to derive an LST pattern that is 10 times finer than the MODIS\LST band (1000 m), t which is agreed on by different researchers, that thermal sharpening can be applied to target 4–16 times of thermal band resolutions. (Essa et al., 2017; Agam et al., 2007b). For statistical downscaling methods like DisTrad, a wide data range of values of SIs and LST are crucial for developing robust regression models. (Essa et al., 2017; Agam et al., 2007b; Kustas et al., 2003). Resultantly, a wide data range of heterogeneous land covers (SIs) and sunny conditions (LSTs) can be more effective in the DisTrad thermal sharpening technique (Essa et al., 2017; Agam et al., 2007b). We argue that arid and semi-arid climates are the typical environment for thermal sharpening. In this study, a coarse resolution of LST (1000 m simulating MODIS\LST image) is sharpened to target 100 m resolution, over different land cover scenarios of the Gaza Strip. For a detailed review of the DisTrad procedure, the reader is referred to Kustas et al. (2003) and Essa et al. (2012).

Downscaling Experiment

Typically, DisTrad sharpened LST higher-resolution (HR) products need to be evaluated with observed HR LST data acquired at the same moment and on the same image. However, when using observed (HR) from different sensors, "it differs in acquisition time and date, data level, processing algorithms, temporal integration, geometric accuracy, etc." (Essa et al., 2017). Therefore, in our study, the thermal and multispectral bands of the Landsat\8 image were aggregated by spatial averaging to a lower resolution (LR) image of 1000 m (simulating MODIS sensor). In this method, DisTrad was used to sharpen LR LST data (1000 m) to target HR image (100 m), "the performance of Dis-

Trad can be optimized and verified in a best-case scenario, independent of errors introduced by differences between sensors" (Essa et al., 2017). Simulation of LST (LR) at 1000 m resolution was crucial because real LST images have sensor registration noise. SIs images (HR), land cover classification map (HR), and LST (LR) images are all from the same sensor and same image (Landsat\8). The sharpened LST products (100 m) are validated by comparing them with the observed Landsat\LST image at the HR (100 m). The 21 SIs and the Landsat 8\LST (band10) were aggregated to simulate the observed data by using spatial averaging to LR images (1000 m). Several studies used the spatial averaging procedure to simulate observed remote sensing data. For Example, Dominguez et al. (2011) simulated ASTER LST LR data (90 m) from HR albedo, NDVI, and LST (10 m) to evaluate the HUTS thermal sharpening method. Agam et al. (2007b) simulated ASTER LST LR data (90 m) from HR NDVI and LST (10 m) to evaluate the TsHARP method (Agam et al., 2007a, 2007b). Essa et al. (2017) simulated MODIS daily LST (960 m) from HR Impervious percentage index and NDVI (30 m) to evaluate the DisTrad method (Kustas et al., 2003). In this study, the Landsat 8 HR data including 21 SIs (30 m) and LST data (100 m) aggregated to LR 1000 m images to simulate MODIS daily LR LST (960 m). Consequently, the DisTrad method was used to sharpen the LR images to target the HR LST image (100 m), for evaluation of DisTrad at the HR (100 m). The downscaled and observed images were compared (Figure. 3).

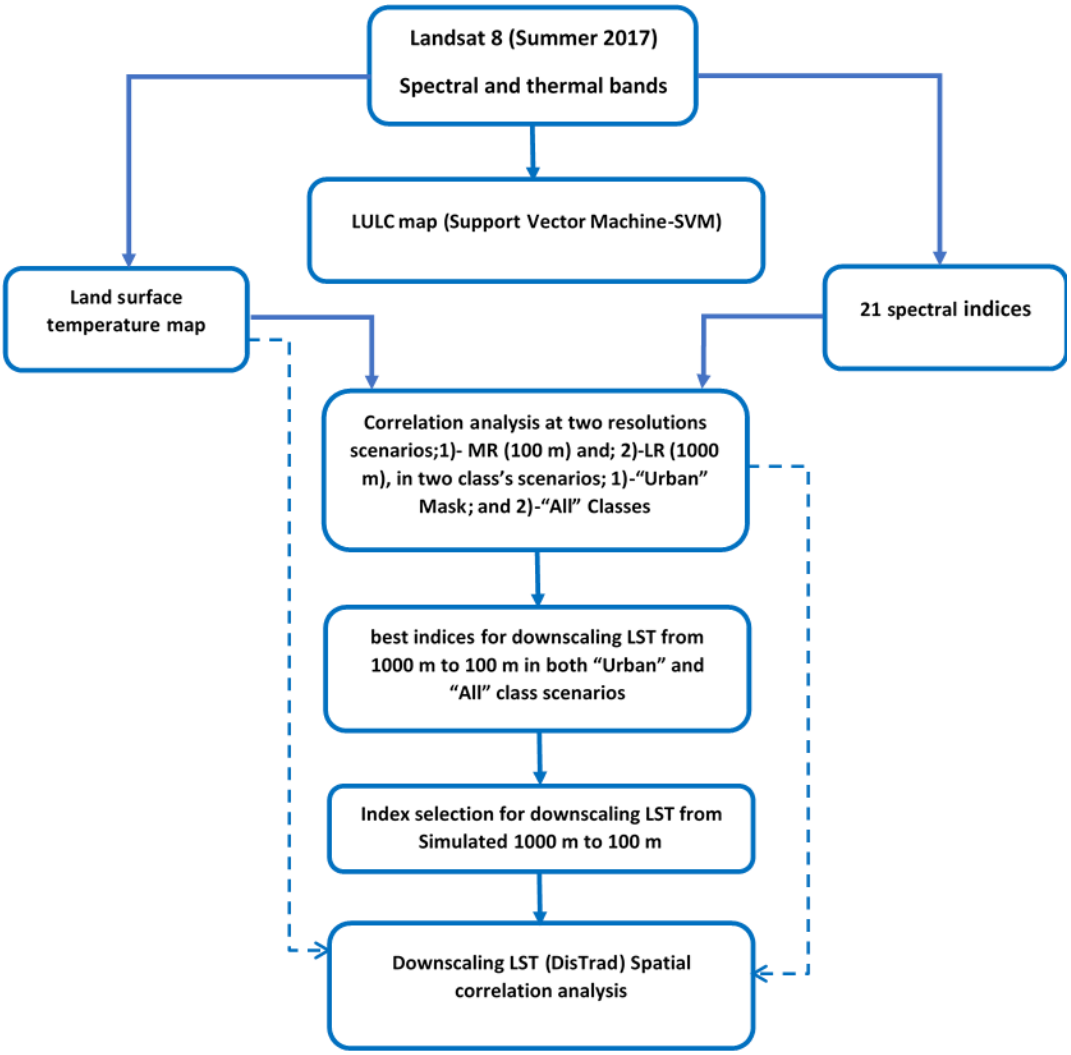

Figure (3): The flowchart showing the procedure and the methodology for evaluating 21 spectral indices for downscaling land surface temperature. The flowchart includes the procedure of regression analysis and the spatial correlation..

Results and discussion

Spectral indices (SIs) vs. L8 LST at 100 m and 1000 m resolutions

The regression analysis between LSTs and SIs was investigated and evaluated in two class-based scenarios including the urban mask (table. 3+4), and All classes (table. 5+6). Moreover, the scale dependency was also evaluated at two scales; 1) at 100 m, which corresponds to middle-resolution (MR) sensors such as Landsat sensors series, and 2) at 1000 m resolution, which corresponds to low-resolution (LR) sensors. Table (3) shows the correlation analysis between SIs and LST for the "urban" class at the LR scale. The robustness of SIs for estimating LSTs shows a higher correlation (R^2) with a lower RMSE error, as it is described in table (3) to follow the SIs order; Dry Bare-Soil Index - DBSI (0.64; 1.18), Built-up Area Extraction Index - BAEI (0.57; 1.28), Bare Soil Index - BSI (0.56; 1.30), Normalized Difference Built-Up Index - NDBI (0.46; 1.43), etc., respectively. Although other SIs show a lower correlation with LST, they still possess valuable information for un-mixing urban LST. Integration of SIs using multiple linear regression may lead to a better estimation of urban LSTs within the land cover class. The SIs equations in the table (2) reveal the robustness of the impervious cover (ABEI, NDBI, BAEI, etc.) and bare soil (DBSI,

BSI, etc.) for characterizing the thermal environment. Those indices were found most representative at the LR scale because of built-up and bare soil covers in arid and semi-arid regions that have similar spectral signatures and thermal properties. The equations of SIs (table 2) reveal the importance of spectral bands such as the green band (GREEN), the red band (RED), the near-infrared band (NIR), and the short-wave infrared (SWIR1) for characterizing LST in arid and semi-arid environments. The SIs can successfully characterize the spectral response of built-up cover and the corresponding LSTs at the LR scale.

Table (*3*). Correlation coefficients and goodness of fit for the correlation between observed land surface temperature (LST) and the 21 spectral indices (SIs) calculated for "urban" class at 1000 m resolution.

Regression Statistics				Correlation LST and SIs				
Index ID	**Mean**	**Std. Dev.**	**Median**	**a**	**bx**	**cx^2**	**R^2**	**RMSE**
DBSI	35.13	1.57	34.68	35.828	-50.358	280.09	0.64	1.18
BAEI	35.13	1.49	34.76	98.651	-95.487	34.763	0.57	1.28
BSI	35.13	1.47	34.74	37.626	-97.097	611.67	0.56	1.30
NDBI	35.13	1.34	34.77	35.273	54.642	518.65	0.46	1.43
BI	35.13	1.18	34.92	32.244	2.7683	51.243	0.36	1.56
UI	35.13	1.18	34.84	45.318	23.057	11.692	0.36	1.56
NBI	35.13	1.17	34.94	27.752	37.701	-14.375	0.35	1.57
VIBI	35.15	1.16	35.11	46.955	-15.482	4.1604	0.35	1.56
IBI	35.13	1.15	34.93	34.859	117.18	2793	0.34	1.59
ABEI	37.86	0.86	37.87	24.653	-822.45	-11186	0.30	1.31
BRBA	35.13	0.92	35.18	58.425	-52.598	27.245	0.22	1.73
NDSI	35.19	0.91	34.99	35.241	23.761	112.31	0.22	1.72
MSAVI2	35.13	0.88	35.55	-50.448	170.07	-83.866	0.20	1.75
ENBI	35.13	0.88	35.48	35.6	0.5688	-0.2085	0.20	1.75
P_Imp	35.13	0.88	35.47	33.721	1.4858	-0.2501	0.20	1.75
NBUI	35.13	0.82	34.94	68.056	190.31	267.18	0.17	1.78
SAVI	35.13	0.72	35.44	28.038	209.88	-1432.7	0.13	1.82
VgNIR-BI	35.13	0.60	35.41	20.513	-75.687	-94.95	0.09	1.86
NDVI	35.13	0.58	35.39	29.251	61.967	-150.24	0.09	1.87
VrNIR-BI	35.13	0.58	35.39	29.251	-61.967	-150.24	0.09	1.87
BUI	35.13	0.48	35.35	34.784	-8.9841	-29.701	0.06	1.90

***Table* (*4*):** Correlation coefficients and goodness of fit for the correlation between observed land surface temperature (LST) and the 21 spectral indices (SIs) calculated for "urban" class at 100 m resolution.

Regression Statistics				Correlation LST and SIs				
Index ID	**Mean**	**Std. Dev.**	**Median**	**a**	**bx**	**cx^2**	**R^2**	**RMSE**
MSAVI2	35.27	1.68	35.67	-18.891	108.45	-53.541	0.50	1.68
P_Imp	35.27	1.54	35.71	26.25	4.3977	-0.4936	0.42	1.81
BAEI	35.31	1.16	35.27	56.248	-24.743	5.7215	0.33	1.65
NBI	35.26	1.37	35.60	21.49	104.86	-181.82	0.33	1.95
ABEI	35.33	1.01	35.02	34.652	-68.465	2984	0.31	1.50
BSI	35.28	1.09	35.33	32.895	4.1236	134.38	0.23	1.99
IBI	35.26	1.09	35.46	29.469	-177.94	-947.62	0.21	2.11
DBSI	35.26	1.09	35.14	33.712	-6.93	108.29	0.21	2.12
NDSI	35.26	0.88	35.04	35.53	41.243	377.29	0.14	2.21
NDBI	94.21	25.31	35.47	35.272	0.83	35.26	0.12	2.23
UI	35.26	0.77	35.31	39.142	7.1801	2.2602	0.10	2.25
ENBI	35.26	0.72	35.58	33.11	1.8125	-0.3044	0.09	2.27
BI	35.26	0.69	35.20	45.939	-20.322	7.6878	0.08	2.28
SAVI	35.33	0.52	35.53	32.618	81.447	-519.96	0.08	1.73
BRBA	35.26	0.66	35.22	43.338	-13.465	3.2237	0.08	2.28
VgNIR-BI	35.32	0.54	35.52	27.118	-44.098	-55.835	0.08	1.87
NDVI	35.33	0.44	35.48	33.087	24.198	-55.765	0.06	1.76
VrNIR-BI	35.33	0.44	35.48	33.087	-24.198	-55.765	0.06	1.76
NBUI	35.26	0.53	35.15	46.133	55.197	65.793	0.05	2.32
BUI	35.33	0.33	35.45	35.273	-2.9624	-10.45	0.03	1.78
VIBI	35.27	0.26	35.29	35.652	-0.328	-0.0114	0.01	2.37

Table (4) shows the correlation analysis between SIs and LST for the "urban" mask at the MR scale (100 m). The best SIs with higher correlation (R^2) and a lower RMSE error is to follow the SIs order; Modified Soil-Adjusted Vegetation Index - MSAVI2 (0.50; 1.68), Impervious Fraction - P_imp (0.42; 1.81), Built-up Area Extraction Index - BAEI (0.33; 1.65), New Built-Up Index - NBI (0.33; 1.95), etc., respectively. The SIs were found to be successfully characterizing the LST at the MR scale. MSAVI2 shows to have the highest correlation because bare soil in arid and semi-arid areas is the most dominant land cover and has the greatest contribution to the thermal budget.

Even though SIs such as DBSI, BAEI, BSI, and NDBI have the highest correlation at LR scales (table 3), they are shifted backward in correlation (table 4) behind MSAVI2 and P_imp at the MR scale (100 m). Moreover, both indices MSAVI2 and P_imp show the highest correlation at the MR scale; however, they possess a lower correlation (R^2=0.20) at the LR scale.

Table (5) shows the correlation analysis between SIs and LST for the "All" class at the LR scale (1000 m). The most robust SIs for estimating LSTs shows a higher correlation (R^2) with a lower RMSE error described to follow the order; DBSI (0.66; 1.22), ABEI 0.59; 1.35), BSI (0.56; 1.40), BAEI (0.47; 1.54), NDBI (0.43; 1.59), etc., respectively. The equations of those SIs are indicated in the table (2) revealing the robustness of the spectral bands used to calculate the impervious cover (ABEI, NDBI, BAEI) and bare soil cover (DBSI, BSI) for controlling the thermal environment in the mixed land cover environment at low resolution (1000 m), in arid and semi-arid climate areas like the Gaza Strip.

Table (6) shows the correlation analysis between SIs and LST for the "All" class at the MR scale (100 m). The best SIs for estimating LSTs with a higher correlation (R^2) and a lower RMSE error described to follow the SIs order; DBSI (0.58; 1.57), ABEI (0.52; 1.69), BSI (0.49; 1.73), BAEI (0.44; 1.83), NDBI (0.40; 1.89), etc., respectively. Those SIs revealed the robustness of impervious cover (ABEI, NDBI, BAEI) and bare soil cover (DBSI, BSI) for controlling the thermal environment in the mixed land cover environment at 100 m resolution, in areas with the arid and semi-arid climate like the Gaza Strip. Those SIs with higher correlation has maintained the highest correlation and the lowest RMSE errors among other indices at the two analyzed scales (1000 m and 100 m). However, the correlation (R^2) and RMSE error slightly enhanced at the LR scale (Table 5) than the MR scale (Table 6), which reveals the scale independence relationship between those indices and land surface temperature. Scale independence is critical for better performance of thermal downscaling techniques such as DisTrad to produce higher-quality and higher-resolution LST patterns.

Table (*5*). Correlation coefficients and goodness of fit for the correlation between observed land surface temperature (LST) and the 21 spectral indices (SIs) calculated for all classes "All" at 1000 m resolution.

Regression Statistics				Correlation LST and SIs				
Index ID	Mean	**Std. Dev.**	**Median**	**a**	**b*x***	**c*x*^{2}**	**R^2**	**RMSE**
DBSI	36.15	1.72	35.83	33.32	-5.2191	126.94	0.66	1.22
ABEI	36.15	1.62	36.04	33.931	-58.125	4127.3	0.59	1.35
BSI	36.15	1.58	35.87	34.614	-22.831	274.54	0.56	1.40
BAEI	36.15	1.45	36.07	72.299	-50.052	15.677	0.47	1.54
NDBI	36.15	1.39	35.94	36.402	40.158	209.4	0.43	1.59
BI	36.15	1.24	36.05	32.09	16.513	12.789	0.34	1.71
NBI	36.15	1.23	36.09	28.066	46.507	-41.036	0.34	1.72
IBI	36.15	1.22	36.06	33.184	-22.102	1062.8	0.33	1.72
UI	36.15	1.18	35.95	42.605	13.093	5.4214	0.31	1.75
BRBA	36.15	0.97	36.54	28.725	37.765	-40.03	0.21	1.87
NBUI	36.15	0.97	36.38	48.493	50.632	25.691	0.21	1.88
MSAVI2	36.16	0.94	36.55	-90.689	249.32	-122.05	0.20	1.89
NDSI	36.21	0.94	36.12	36.282	17.776	51.639	0.20	1.88
ENBI	36.15	0.91	36.52	34.446	2.0473	-0.4904	0.19	1.90
P_Imp	36.15	0.91	36.51	29.21	4.1238	-0.5771	0.19	1.90
SAVI	36.15	0.86	36.51	26.566	259.82	-1661.7	0.16	1.93
VgNIR-BI	36.15	0.77	36.46	11.713	-121.89	-148.75	0.13	1.96
BUI	36.15	0.75	36.28	37.605	3.6822	-8.2808	0.13	1.97
VIBI	36.15	0.75	36.23	38.198	-1.5097	-0.304	0.12	1.97
NDVI	36.15	0.73	36.43	29.527	66.463	-154.61	0.12	1.98
VrNIR-BI	36.15	0.73	36.43	29.527	-66.463	-154.61	0.12	1.98

Table (6): Correlation coefficients and goodness of fit for the correlation between observed land surface temperature (LST) and the 21 spectral indices (SIs) calculated for all classes "All" at 100 m resolution.

Regression Statistics				Correlation LST and SIs				
Index ID	**Mean**	**Std. Dev.**	**Median**	**a**	**b*x***	**c*x*^{2}**	**R^2**	**RMSE**
DBSI	36.83	1.85	36.61	33.535	9.747	51.116	0.58	1.57
ABEI	36.83	1.75	36.67	34.627	-75.408	2444.4	0.52	1.69
BSI	36.83	2.42	36.69	33.75	15.18	70.625	0.49	1.73
BAEI	36.83	1.60	36.81	64.486	-36.876	10.669	0.44	1.83

Regression Statistics			
Index ID	**Mean**	**Std. Dev.**	**Median**
NDBI	36.83	1.54	36.89
NDSI	36.83	1.50	36.64
NBI	36.83	1.34	36.96
IBI	36.83	1.34	36.86
UI	36.83	1.29	37.01
NBUI	36.83	1.10	36.97
VgNIR-BI	36.83	1.03	37.26
BUI	36.83	0.97	37.05
ENBI	36.83	0.89	37.19
P_Imp	36.83	0.93	37.19
BI	36.83	0.87	37.00
BRBA	36.83	0.87	37.00
MSAVI2	36.83	0.73	37.11
NDVI	36.83	0.81	37.09
VrNIR-BI	36.83	0.81	37.09
SAVI	36.83	0.72	37.03
VIBI	36.83	0.28	36.84

Correlation LST and SIs				
a	**b*x***	**cx^2**	**R^2**	**RMSE**
37.029	26.998	52.258	0.40	1.89
37.029	26.998	52.258	0.38	1.91
30.421	39.249	-40.979	0.31	2.03
33.778	-54.432	369.06	0.31	2.03
39.709	4.2676	0.485	0.28	2.07
45.913	38.986	24.217	0.21	2.17
21.044	-267.987	-94.51	0.18	2.20
38.489	6.9931	0.7465	0.16	2.23
35.936	1.2654	0.2978	0.15	2.25
32.879	2.4558	-0.3427	0.15	2.25
45.38	-15.224	3.2162	0.13	2.27
45.37	-15.205	3.2086	0.13	2.27
-4.8562	78.327	-36.374	0.12	2.29
35.069	20.186	-47.365	0.11	2.29
35.071	-20.182	-47.365	0.11	2.29
34.701	58.904	-356.29	0.09	2.33
37.005	-0.1569	-0.0004	0.01	2.42

Best SIs – LST relationship in Urban and "All" classes

For the urban class, the scatterplots of SIs have the highest correlation with LST shown at the LR scale (Fig. 4) and MR scale (Fig. 5). The statistical fitting shows that second-order polynomial fit best describes the SIs-LST relationships and proves to have a better R^2 than other statistical fits like the linear regressions because of that polynomial fit was selected for our analysis.

Figure (4) shows the scatterplots for the SIs at the LR scale (1000 m) for the "Urban" class. At the lower-middle DBSI values (Fig. 4a), bare soil and built-up areas are mixed because of the low resolution, which results in a wide LST range due to the cooling and moderating effect of shading effects of high built-up constructions within the urban area (cities center). While DBSI increases, especially at the city peripheries where a smaller fraction of the building covering the pixels exists at LR scale (1000 m), the LST range decreases but increases in value because of the warming effects of pure bare soil pixels due to its thermal physical properties. The contribution of bare soil is nearly equal to the built-up contribution (Rasul et al., 2015). BSI index shows a similar scatter with the DBSI index (Fig. 4c). However, for the BAEI index (Fig. 4b), LST has a wide range along the fitting line due to the shading effects of built-up areas in general. When the BAEI increases (e.g., the central part of the cities), the LST value decreases because of the cooling effects of built-up areas by the shading effect. NDVI does not correlate with LST in the Gaza Strip, the scatterplot (Fig. 4d) shows a wide range of LST values and dominates most of the middle part of the NDVI because vegetated area (described as a shrubs, trees, and crops) exists in bare land areas and rarely exist in the urban area, urban areas of the Gaza Strip are charactered by the higher intensity of urbanization and the low green spaces.

Figure (5) shows the scatterplots of SIs at the MR scale (100 m) for the "Urban" class. MSAVI2 (Fig. 5a) showed a wide range of LST values, from both tails of the scatterplot towards the middle part of index values (around 1). Variability in LST values is due to the different shading rates, the physical-thermal properties of the built-up forming materials, and the percentage of bare soil, vegetation, and wetness. Values ranged increases by the higher pixel resolution at ML scale (100 m). The LST narrow range and low values at the lower tails of MSAVI2 values are due to the high cooling and moderating effect of shading (cities Center). The LST wide range and high values in the middle part of MSAVI2 values (around 1) are due to the higher percentage of bare soil, especially in the peripheries. P_imp index (Fig.5b) shows a similar scatterplot as MSAVI2. Similar P_imp pixel values have different LST value because of their various physical and thermal properties and the cooling effects of built-up areas by the shading.

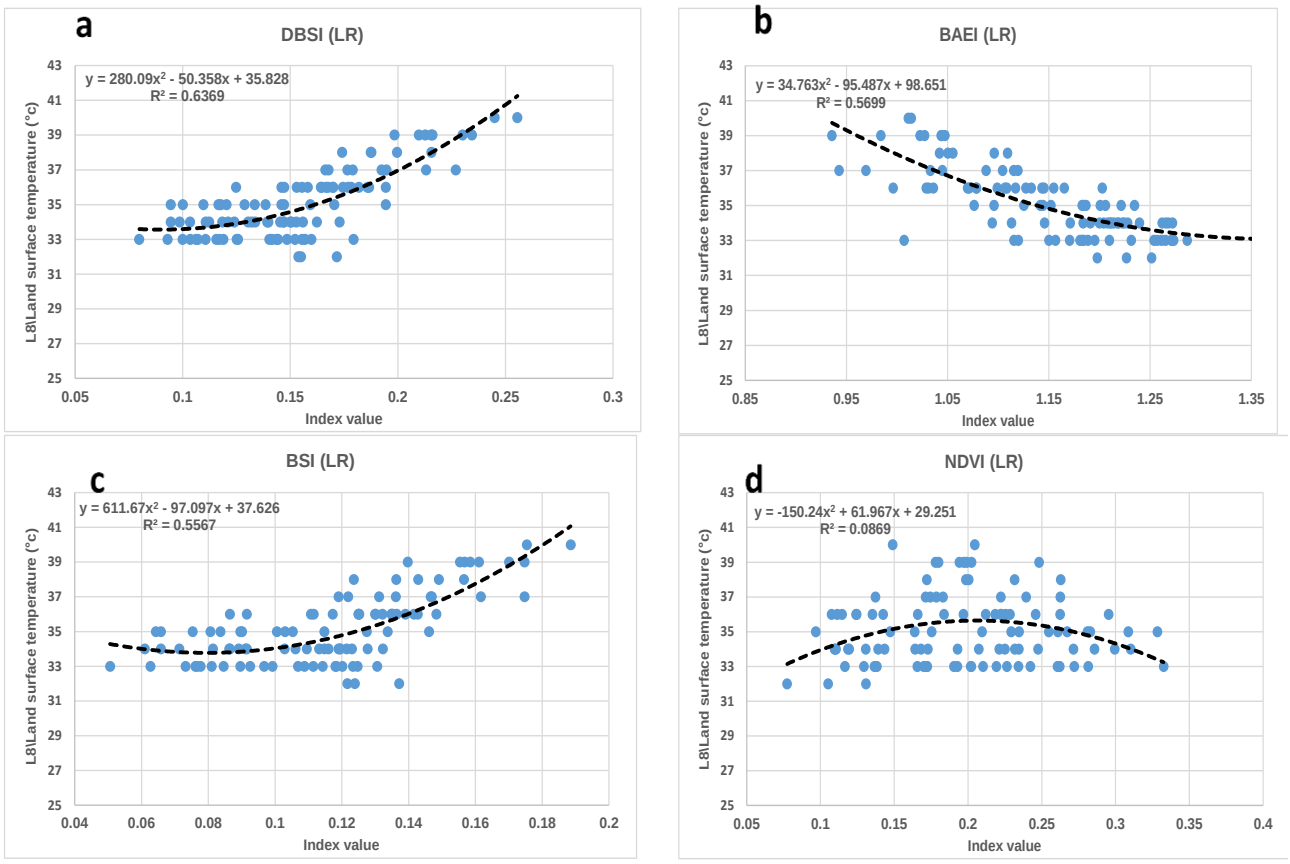

Figure *(4)*: Scatterplots of spectral indices vs observed Landsat 8\land surface temperature for the "urban" class at LR scale (1000 m), using the second order polynomial fitting model.

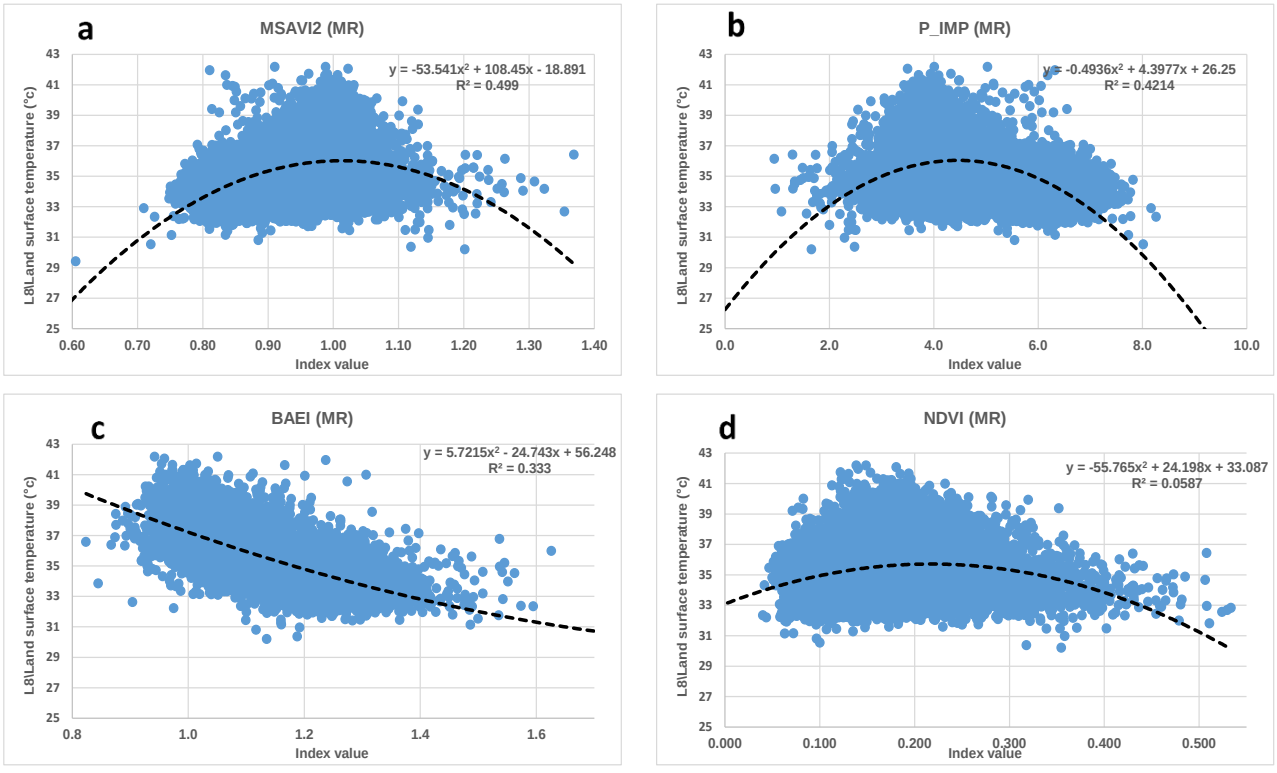

Figure (5): Scatterplots of spectral indices vs observed Landsat 8\land surface temperature for the "urban" class at MR scale (100 m), using the second order polynomial fitting model.

Own et al. (1998) suggested a new approach based on satellite remote sensing data. If a triangular-shaped envelope of pixels is formed in urban areas (like MSAVI2 and P_imp indices) when bare soil experiences a wide variation in LST than densely vegetated locations (referred to as the "triangle method"). Then, “the surface radiant temperature response along the abscissa is a function of varying vegetation cover and surface soil water content” (Own et al., 1998). BAEI index (Fig. 5c) shows a negative relationship with LST, the low BAEI index values are found in urban peripheries, while the high BAEI index values indicate the urban centers. Comparing the NDVI scatterplot (Fig. 5d), NDVI shows no correlation at the MR scale, however, the trend line indicated a shorter and lower LST range at the highest part of the NDVI, which is related to vegetated areas existing in bare soil pockets or urban farming spaces within the urban mask.

Figure (6) shows the scatterplots for the SIs at the LR scale (1000 m) for the “All” class. Both indices DBSI (Fig. 6a) and BSI (Fig. 6c) show similar scatters as the "urban" class (Fig. 4), the middle part of the SIs, LST has a wide range due to the cooling and moderating effect of built-up shading effects. When, DBSI and BSI increase in value because of integrating the bare soil and dune within the regression space, especially the terminal part of urban blocks pixels, LST increases because of the warming effects of the bare soil and dunes' thermal and physical properties. The BAEI index (Fig. 6b) shows similar results as in the "urban" class, LST has a wide range along the fitting line due to the shading effects of built-up areas. When the BAEI increases, the LST value decreases because of the cooling effects of built-up areas by the shading effect. NDVI scatterplot (Fig. 6d) still has a lower R^2 (0.12), however, the R^2 is significantly increased from the "urban" class (0.08) due to integrating other vegetation classes such as trees, crops, greenhouses, and shrubs within the regression analysis.

Figure (7) shows the scatterplots for the SIs at the MR scale (100 m) for the “All” class. Both SIs, the DBSI (Fig. 7a) and the BSI (Fig. 7c) show a similar scatter like in Figure 6. The lower tail of the plot shows low index values in regression space due to adding the vegetation classes in the regression analysis, causing a decrease in the LST value due to the cooling and moderating effect of vegetation classes. DBSI and BSI increase in value because of integrating the pure bare soil and dune classes within the regression analysis, which increases the LST values. The ABEI index (Fig. 7b) shows a similar result to Figure (6b). According to the ABEI (Firozjaei et al., 2019b), “pixels with a value greater than zero are built-up areas, and pixels with values less than zero are non-built-up areas”. Built-up areas showed lower LST values and a narrow value range than the non-built-up area due to the shading effects. In ABEI, vegetation (NDVI > 0.5) is classified into the non-built-up class. The scattered pixels, with ABEI, are greater than ≈0.03 and belong to the vegetation class, averaged LST values are due to vegetation cooling. Negative BAEI values show higher LST values decrease because of the warming effects of bare soil and dunes. Moreover, the NDVI scatterplot (Fig. 7d) shows a similar correlation (R^2=0.11) as in Figure (6.d) (R^2 = 0.12) by integrating vegetation classes into the regression analysis.

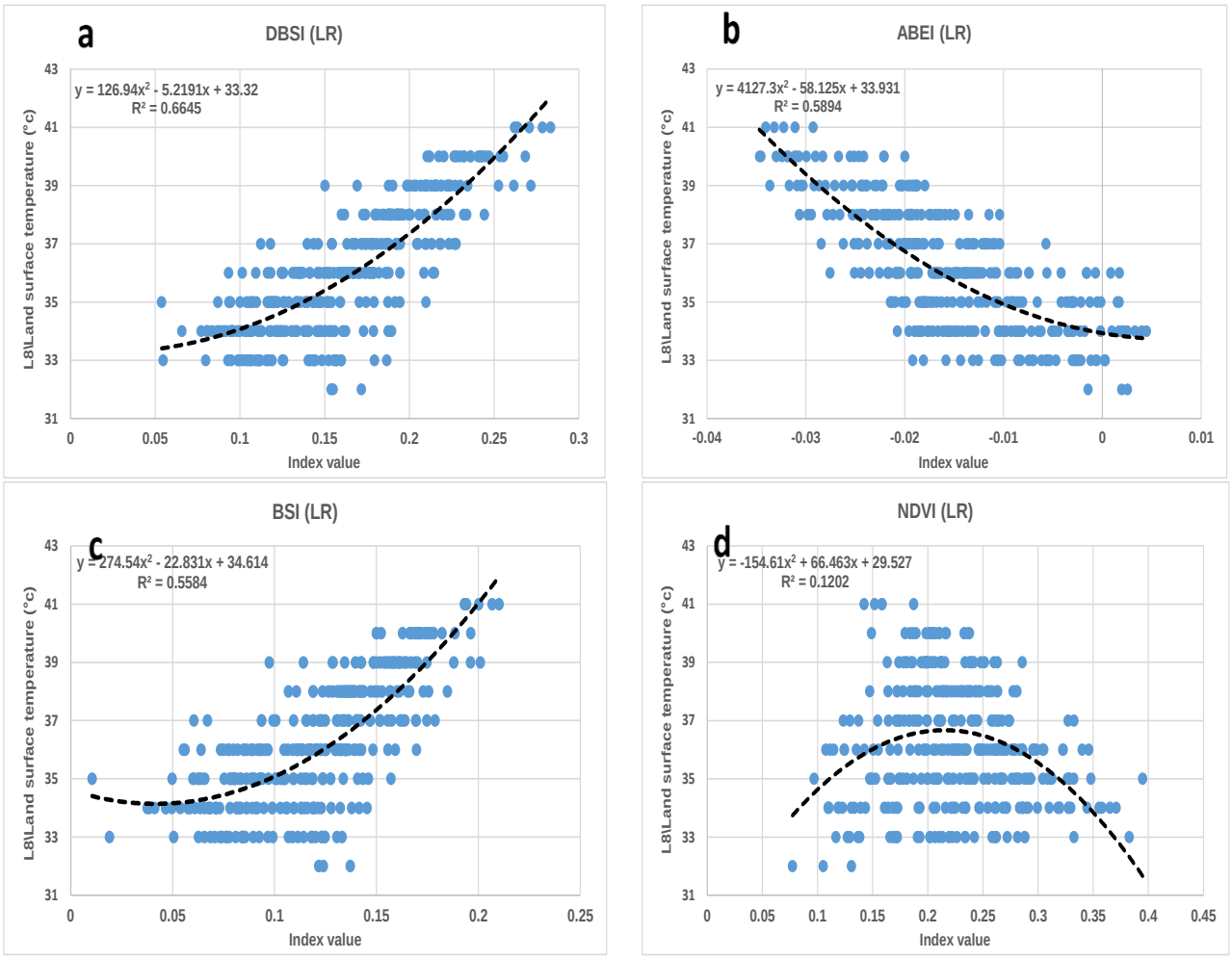

Figure (6): Scatterplots of spectral indices vs observed Landsat 8\land surface temperature for the “All” class at LR scale (1000 m), using the second order polynomial fitting model.

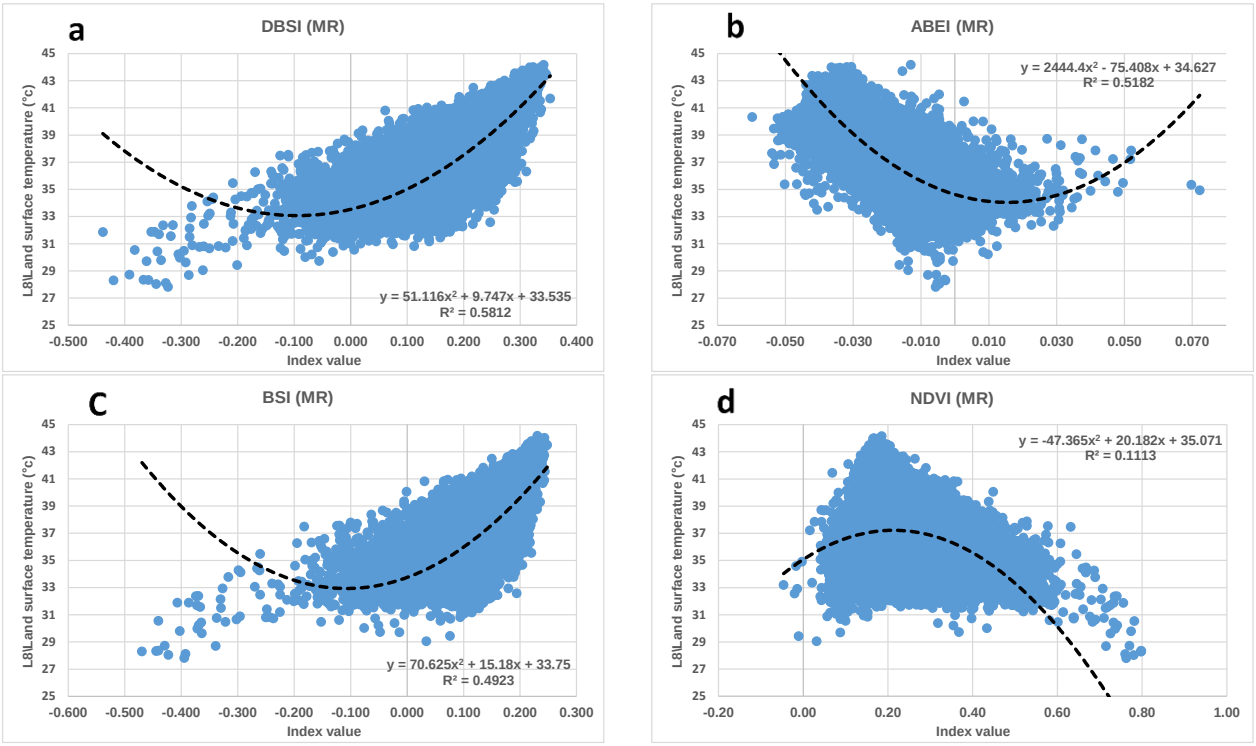

Figure (7): Scatterplots of spectral indices vs observed Landsat 8\land surface temperature for the "All" class at MR scale (100 m), using the second order polynomial fitting model.

DisTrad Thermal Sharpening Results

Based on the correlation coefficient and the scatterplots of each SIs at the LR scale (1000), the SIs; DBSI, ABEI, BSI, BAEI, and NDBI are selected for the thermal sharpening in the "All" classes as in Eq. (1-5) respectively, and the SIs; DBSI, BAEI, BSI and NDBI in the "Urban" class as in the Eq. (6-9) respectively. DisTrad thermal sharpening technique applied for downscaling a simulated MODIS\LST image (aggregated Landsat 8 TIR image to 1000 m) to 100 m resolution using the regression models (Eq. 1-9) within "All" classes and "Urban" class.

$$\mathrm{LST}_{all\_classes} = 126.94\ (\mathrm{DBSI})^2 - 5.2191(\mathrm{DBSI}) + 33.32$$

Equation 1

$$\mathrm{LST}_{all\_classes} = 4127.3\ (\mathrm{ABEI})^2 - 58.125(\mathrm{ABEI}) + 33.931$$

Equation 2

$$\mathrm{LST}_{all\_classes} = 274.54\ (\mathrm{BSI})^2 - 22.831(\mathrm{BSI}) + 34.614$$

Equation 3

$$\mathrm{LST}_{all\_classes} = 15.677(\mathrm{BAEI})^2 - 50.052\ (\mathrm{BAEI}) + 72.299$$

Equation 4

$$\mathrm{LST}_{all\_classes} = 209.4(\mathrm{NDBI})^2 + 40.158\ (NDBI) + 36.402$$

Equation 5

$$\mathrm{LST}_{Urban} = 280.09\ (\mathrm{DBSI})^2 - 50.358(\mathrm{DBSI}) + 35.828$$

Equation 6

$$\mathrm{LST}_{Urban} = 34.763(\mathrm{BAEI})^2 - 95.487\ (\mathrm{BAEI}) + 98.651$$

Equation 7

$$\mathrm{LST}_{Urban} = 611.67\ (\mathrm{BSI})^2 - 97.097(\mathrm{BSI}) + 37.626$$

Equation 8

$$\mathrm{LST}_{Urban} = 518.65(\mathrm{NDBI})^2 + 54.642\ (NDBI) + 35.273$$

Equation 9

The statistics and spatial correlation coefficients between the estimated and observed LST for the "ALL" classes are summarized (Table. 7). Correlation (R^2) and RMSE show better performance when using; Automated Built-Up Extraction Index (ABEI) model (Eq.2), Dry Bare-Soil Index (DBSI) model (Eq.1), and Built-up Area Extraction Index (BAEI) model (Eq.4) show the highest correlation (R^2 = 0.77, 0.73, and 0.70 respectively) with lowest RMSE errors (1.24, 1.47, and 1.43 respectively). ABEI demonstrated its effectiveness to extract built-up areas from other land covers such as bare soil and sandy soil areas where other indices experience significant challenges (Firozjaei et al., 2019b). This study confirms that ABEI successfully can also characterize LST when mixed LULC-like bare and sandy soils with the built-up areas better than other indices (DBSI, BAEI, NDBI, and BSI) in arid and semi-arid climate regions. The ABEI shows to perform better than other SIs of two-band indices or single-band thresholding (Firozjaei et al., 2019b). The "dry bare-soil index (DBSI)" is a newly proposed index by Rasul et al. (2018) to map built-up and bare areas in a dry climate from Landsat 8 in the city of Erbil, Iraq. "DBSI can be used reliably for differentiating constructed and bare land from other land use classes in arid and semi-arid climates" (Rasul et al., 2018). In this study, DBSI shows a high correlation with LST and robust surface parameters for thermal downscaling methods. "Built-up Area Extraction Index (BAEI)" is proposed by Bouzekri et al. (2015) for highlighting built-up areas in the Landsat-8 image, BAEI is characterized by not only using spectral bands but also

introduces arithmetic constant (0.3) to facilitate the extraction of the built-up area. "Visual analysis of extracted spectral indices shows that BAEI gives significant results better than NDBI for highlighting built-up areas in the image" (Bramhe et al., 2018).

"The Normalized Difference Built-up Index (NDBI)" was proposed in 2003 for Nanjing City (Zha et al., 2003), as a method to map built-up areas automatically. The index was also applied by Firozjaei et al. (2019b) in Iranian and European cities. NDBI index was successful to distinguish between built-up and vegetated or green and wet surroundings for Nanjing City. However, "NDBI was not successful in distinguishing between built-up and other land covers such as bare and dry soil that surround Nanjing City, due to the overlapping spectral reflectance for these land cover types" (Firozjaei et al., 2019a; He et al., 2010). Generally, "NDBI is more efficient in places where the NDVI value is greater than 0" (Zha et al., 2003). Although the NDBI show weaknesses in land cover classification for cities located in dry climates, however, it shows a higher correlation with LST in arid and semi-arid climate areas.

Table (7): Statistical characteristics and correlation analysis (R^2 and RMSE) between observed Landsat 8\LST and sharpened LST products based on the different indices calculated within the "All" classes (urban, vegetation, and sandy and bare soil).

Spectral Index	Statistics			Corr. LST and index	
	Mean	Std. Dev.	Median	R^2	RMSE
ABEI	36.79	2.53	36.43	0.77	1.24
DBSI	36.77	2.84	36.30	0.73	1.47
BAEI	36.74	2.55	36.61	0.70	1.43
NDBI	36.77	2.83	36.41	0.54	1.94
BSI	36.73	3.12	36.19	0.51	2.18

The statistics and spatial correlation coefficients between the estimated and observed LST for the "urban" class are summarized (Table. 8).

The high correlation (R^2) and lowest error (RMSE) values prove when using; Dry Bare-Soil Index (DBSI) (Eq.6) and Built-up Area Extraction Index (BAEI) (Eq.7), the best results are shown with the highest correlation (R^2 = 0.59, and 0.58 respectively) with lowest RMSE errors (1.28 and 1.44 respectively).

Table (8): Statistical characteristics and correlation analysis (R^2 and RMSE) between observed Landsat 8\LST and sharpened LST products based on the different indices calculated within the "Urban" class.

Spectral Index	Statistics			Corr. LST and index	
	Mean	Std. Dev.	Median	R^2	RMSE
DBSI	35.07	1.90	34.77	0.59	1.28
BAEI	35.24	2.23	34.83	0.58	1.44
BSI	35.00	2.14	34.74	0.46	1.65
NDBI	35.01	2.39	34.71	0.40	1.90

Descriptive analysis

The performance of the DisTrad sharpening technique is investigated visually for all the sharpened image products using the models (Equations 2 to 9) for the "All" class and the "urban" class, as shown in figure (8) and figure (9) respectively. Figure (8a) shows the original image of Landsat 8\LST image at 100 m resolution, while Figure (8b) shows the aggregated values of Landsat 8\LST using the average to 1000 m resolution to simulate MODIS LST imagery. Figures (8c-g) are the sharpened products using the indices; NDBI, DBSI, BSI, BAEI, and ABEI, respectively. The absolute error differences of 2°C were calculated (observed image minus sharpened image), using the above indices. The greatest sum of pixels (in percentage) of the downscaled products with the smallest Absolute Error difference (<=2°C) is used as an indicator for downscaling quality. For example, figure (8g) shows the smallest absolute error differences (the green color pixels) for the ABEI model. The best-downscaled products with the smallest absolute error differences (<=2°C) are when using the SIs in order; ABEI (90.9%), BAEI (90.7%), DBSI (85.6%), NDBI (85.3%), and BSI (84.2%). The Large error differences (red pixels in Fig. 8g) are caused by mixed pixels located at the urban class boundary with water bodies, such as beaches and sewage treatment ponds, along the coastal edge, because of that, urban coastal edge pixels need to be masked out. The internal large error differences are caused by the extreme outliers of the original SIs index values.

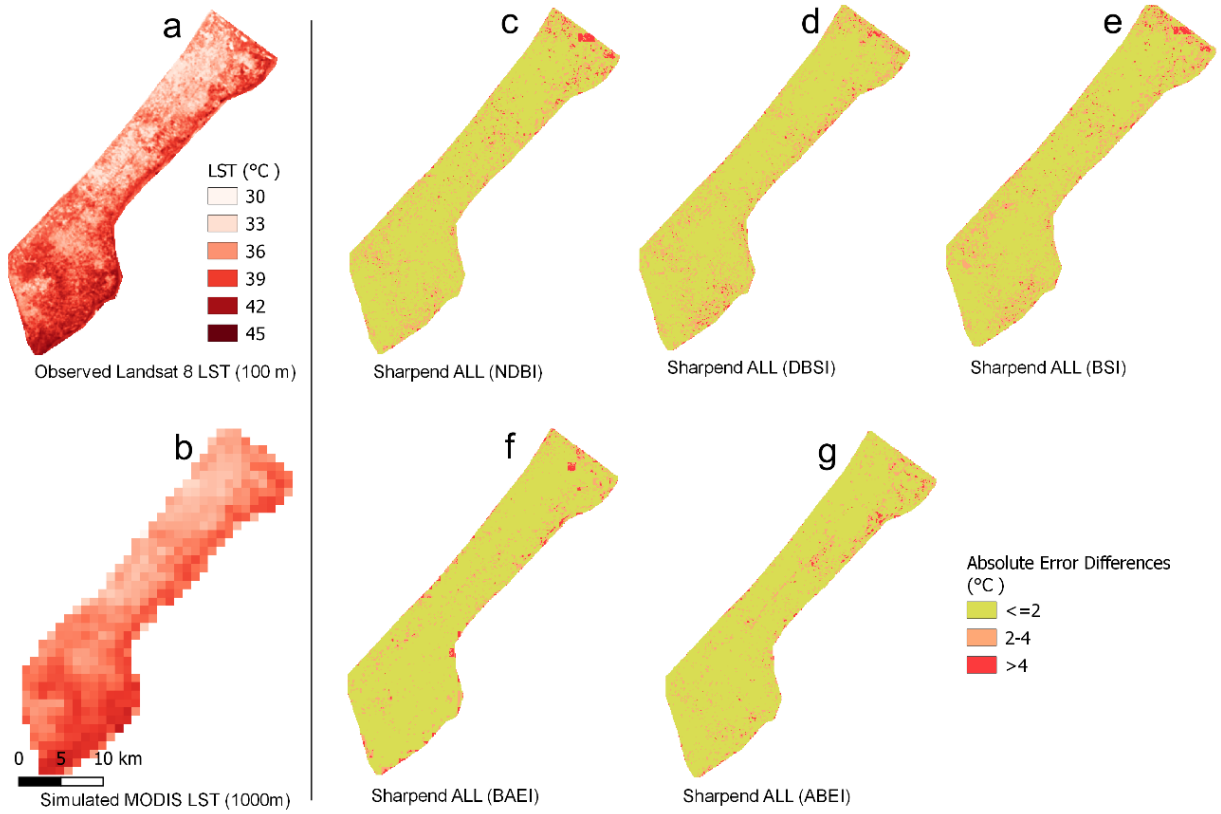

Figure (8): Observed Landsat8\LST-100m (a) and simulated LST-1000m (b) versus the sharpened LST at 100m resolution for the “All” class, based on the indices; NDBI(c), DBSI(d), BSI(e), BAEI(f), and ABEI (g). Absolute error difference calculated by = Observed LST – Sharpened LST using ABEI (h).

Figure (9a) and figure (9b) show the original image of Landsat 8\LST image at 100 m resolution and the simulated MODIS LST image at 1000 m respectively. Figure (9c-f) is the absolute error differences within the "urban" class. The best-downscaled products with the smallest absolute error differences (<=2°C) are shown when using the SIs in order; DBSI (90%), BAEI (86.5%), BSI (86.5%), and NDBI (81.4%). The Large error differences are caused by mixed pixels located at the urban class boundary with other classes, such as bare soil, water bodies, mixed pixels, and land cover misclassification. The mixed pixels are caused by similar spectral characteristics such as the bare soil, sandy areas, and low vegetated areas. Most of these misclassified pixels are seen to be the same pixels in all calculated indices. The large error in estimating LST is because of downscaling applied to SIs indices and its spectral properties. An additional source of downscaling error might be the anthropogenic heat in various forms, which are explicitly incorporated into the energy balance (e.g. heat from transportation, industry, households, etc.). Those pixels with the higher estimating errors were found randomly distributed along with the transportation systems or industrial clusters outside the cities.

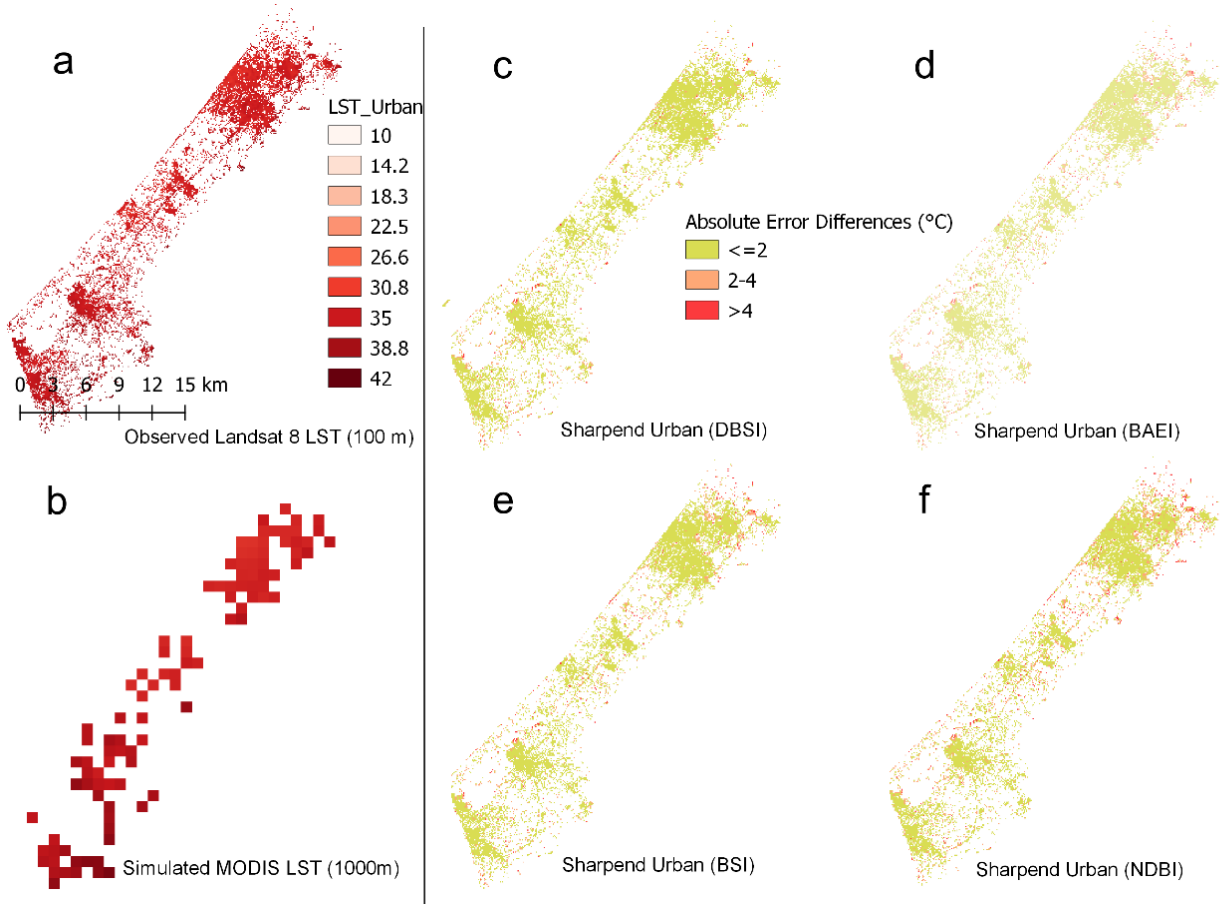

Figure (9): Observed Landsat8\LST-100m (a) and simulated LST-1000m (b) versus the sharpened LST at 100m resolution for the “urban” class, based on the indices; DBSI(c), BAEI(d), BSI(e), and NDBI (g).

Conclusion

The Gaza Strip is located in an arid and semi-arid climate where the urban peripheries are mostly dominated by bare soil that absorbs more heat than the urban area itself, bare soil does not have large evaporation and transpiration effects to mitigate the temperature of the soil. In such a climate, the LST pattern can be generally described as an urban cool island (UCI).

In the urban areas of the Gaza Strip, the spatial distribution of LST shows an inverse relationship between the built-up indices and LST because of the cooling effects of built-up areas shading. However, in the peripheries, LST increases because of the warming effects of the bare soil and dunes' thermal and physical properties.

This research is limited to the spatial variation of the LST in the daytime during the dry season of an arid and semi-arid climate area. Other temporal variations including seasonal, and diurnal might be useful for the validation of SIs - LST relationships within areas that have similar climate types.

The distribution of downscaled LST matched the distribution of urban cool island (UCI) producing a good spatial correlation (R^2) and lower RMSE error with the observed Landsat\LST image. Moreover, the best-downscaled products have been produced in the "All" class when using the following SIs in order; ABEI (90.9%), BAEI (90.7%), DBSI (85.6%), NDBI (85.3%), and BSI (84.2%), and in "urban" class when using the following SIs in order; DBSI (90%), BAEI (86.5%), BSI (86.5%), and NDBI (81.4%).

The correlation analysis between the SIs and LST at the two scales (100 m and 1000 m) reveals the spatial scale dependency for some SIs. In the "urban" class, although both indices (MSAVI2 and P_imp) have the highest correlation at the MR scale (0.50 and 0.42 respectively), they have shown a lower correlation (R^2 =0.20) at the LR scale. Resultantly, MSAVI2 and P_imp are scale-dependent and may not be useful for downscaling LST from 1000 m resolution. They are more suitable to downscale LST from 100 m to higher resolutions (e.g., Landsat 7 ETM+ 60 m resolution). Opposite to MR (100 m), the SIs including DBSI, BSI, BAEI, and NDBI show a higher correlation in the "urban" class at LR (1000 m). That SIs reveals to be scale-dependent parameters. However, they might be useful for downscaling LST to closer resolutions to 1000 m (e.g., 500 m), and further scale dependency analysis might be investigated in different applications.

The best SIs for estimating LSTs for the class "All", which have a higher correlation (R^2) and a lower RMSE error, are in order; DBSI, ABEI, BSI, BAEI, and NDBI. Those indices contribute significantly to the thermal environment of a mixed land cover type. The SIs maintained the highest correlation among other indices at the two analyzed resolutions (100 m and 1000 m), which means those indices are scale independent and perform well in downscaling LST.

Ethics approval and consent to participate.

Not applicable

Consent for publication

Consent for publication is accepted by Essa and Lhissou (2021) for using the LC map (Figure. 2).

Consent for publication is accepted by Essa, W. (2022) for using the table of indices (Table 2).

Availability of data and materials

The raw data of Landsat 8 image required to reproduce the spectral indices and land surface temperature are available online using the Earth Explorer website https://earthexplorer.usgs.gov/

Author's contribution

The authors confirm contribution to the paper as follows: study conception and design: Wiesam ESSA, theoretical calculations and modeling: Wiesam ESSA, Rachid LHISSOU; data analysis and validation, Wiesam ESSA, draft manuscript preparation: Wiesam ESSA, all authors reviewed the results and approved the final version of the manuscript.

Funding

This study is supported by the Palestinian Quebecer Science Bridge (PQSB). MEDRC Water Research Innovation Initiative Award - Palestine I2 Grant Award. https://www.medrc.org/fellowships/

Conflicts of interest

The authors declare that there is no conflict of interest regarding the publication of this article.

Acknowledgments

This study is supported by the Palestinian Quebecer Science Bridge (PQSB)

References

Adnan M. Aish, O. Batelaan and F. De Smedt. Distributed Recharge Estimation for Groundwater Modeling Using WETSPASS Model, Case Study- Gaza Strip, PALESTINE The Arabian Journal for Science and Engineering, Volume 35, Number 1B 1.

Agam, N., Kustas, W.P., Anderson, M.C., Li, F., Colaizzi, P.D. (2007a). Utility of thermal sharpening over Texas high plains irrigated agricultural fields. Journal of Geophysical Research, 112, D19.

Agam, N., Kustas,W.P., Anderson, M.C., Li, F., Neale, C.M.U. (2007b). A vegetation index based technique or spatial sharpening of thermal imagery. Remote Sensing of Environment, 107, 545–558.

Agam, N., Kustas, W.P., Anderson, M.C., Li, F., Colaizzi, P.D. (2008). Utility of thermal image sharpening for monitoring field-scale evapotranspiration over rainfed and irrigated agricultural regions. Geophysical Research Letters, 35, 2.

Agathangelidis, A & Cartalis, C. (2019): Improving the disaggregation of MODIS land surface temperatures in an urban environment: a statistical downscaling approach using high-resolution emissivity, International Journal of Remote Sensing, DOI: 10.1080/01431161.2019.1579386

Bala, R., Prasad, R., Yadav, V.P. (2019). Disaggregation of modis land surface temperature in urban areas using improved thermal sharpening techniques. Advances in Space Research, 64(3),591-602, ISSN 0273-1177, https://doi.org/10.1016/j.asr.2019.05.004.

Bechtel, B, K. Zakšek, and G. Hoshyaripour. (2012). Downscaling land surface temperature in an urban area: A case study for Hamburg, Germany, Remote Sensing., vol. 4, pp. 3184–3200.

Bechtel, B. (2012). Robustness of annual cycle parameters to characterize the urban thermal landscapes. IEEE Geosci. Remote Sensing Letters, 9, 876 –880.

Bindhu, M., Narasimhan, B., Sudheer, K. P. (2013). Development and verification of a non-linear disaggregation method (NL-DisTrad) to downscale MODIS land surface temperature to the spatial scale of Landsat thermal data to estimate evapotranspiration, Remote Sensing of Environment, 135, Pages 118-129, ISSN 0034-4257, https://doi.org/10.1016/j.rse.2013.03.023.

Bouzekri, S., Lasbet, A.A., Lachehab, A. (2015). A new spectral index for extraction of built-up area using landsat-8 data. The Journal of the Indian Society of Remote Sensing, 43, 867–873.

Bramhe, V. S. and Ghosh, S. K. and Garg, P. K. (2018). EXTRACTION OF BUILT-UP AREA BY COMBINING TEXTURAL FEATURES AND SPECTRAL INDICES FROM LANDSAT-8 MULTISPECTRAL IMAGE. ISPRS - International Archives of the Photogrammetry, Remote Sensing and Spatial Information Sciences, XLII-5, 727–733. https://doi.org/10.5194/isprs-archives-XLII-5-727-2018

Congedo, L. (2016). Semi-Automatic Classification Plugin documentation. Release, 225–235. DOI: 10.13140/RG.2.2.29474.02242/1

Coppo, P., Smith, D., Nieke, J. (2015). Sea and Land Surface Temperature Radiometer on Sentinel-3. Optical Payloads for Space Missions, John Wiley & Sons, Ltd.: Hoboken, NJ, USA, pp. 701–714.

DeWitt, J. D., Chirico, P. G., Bergstresser, S. E., Warner, T. A. (2017). Multi-scale 46-year remote sensing change detection of diamond mining and land cover in a conflict and post-conflict setting. Remote Sensing Applications: Society and Environment 2017, 8: 126-139. https://doi.org/10.1016/j.rsase.2017.08.002

Dominguez, A., Kleissl, J., Luvall, J.C., Rickman, D.L. (2011). High-resolution urban thermal sharpener (HUTS). Remote Sensing of Environment, 115, 1772–1780.

Dudeen B. (2001). The soils of Palestine (The West Bank and Gaza Strip) current status and future perspectives. In : Zdruli P. (ed.), Steduto P. (ed.), Lacirignola C. (ed.), Montanarella L. (ed.). Soil resources of Southern and Eastern Mediterranean countries. Bari : CIHEAM, 2001. p. 203-225 (Options Méditerranéennes : Série B. Etudes et Recherches, n. 34)

Essa, W., B. Verbeiren, J. van der Kwast, and O. Batelaan. (2017). Improved DisTrad for Downscaling Thermal MODIS Imagery over Urban Areas. Remote Sensing 9 (12): 1243. doi:10.3390/rs9121243.

Essa, W. (2022). Evaluation of spectral indices for characterizing Urban Cool Island during the dry season from Landsat8; a hot semi-arid climate; case study: of the Gaza Strip. The Journal of Natural Sciences, Al-Aqsa University, 5, 68-89.

Essa, W., Lhissou, R. (2021). Evaluating Built-up Indices for DisTrad Thermal Sharpening over the Arid and Semi-Arid Regions, Case Study: Gaza Strip. LIEGE (BELGIUM) Earth Observation for sustainable cities and communities, 6th EARSel Joint Workshop Urban remote Sensing, 26 – 28 MAY 2021. Liege, Belgium.

Essa, W., Verbeiren, B., van der Kwast, J., Batelaan, O. (2013). Downscaling of thermal images over urban areas using the land surface temperature—Impervious percentage relationship. International Journal of Applied Earth Observation and Geoinformation, 23, 95–108.

Essa, W., Verbeiren, B., van der Kwast, J., Van de Voorde, T., Batelaan, O. (2012). Evaluation of the DisTrad thermal

sharpening methodology for urban areas. International Journal of Applied Earth Observation and Geoinformation. 19, 163–172.

Eswar, R., Sekhar, M., Bhattacharya, B.K. (2016). Disaggregation of LST over India: Comparative analysis of different vegetation indices. International Journal of Remote Sensing, 37, 1035–1054.

Feng, X., Li, J. (2020). Evaluation of the Spatial Pattern of the Resolution-Enhanced Thermal Data for Urban Area", Journal of Sensors, vol. 2020, Article
ID 3427321, 15 pages. https://doi.org/10.1155/2020/3427321

Firozjaei, M.K., Sedighi, A., Argany, M., Jelokhani-Niaraki, M., Arsanjani, J.J. (2019a). A geographical direction-based approach for capturing the local variation of urban expansion in the application of ca-markov model. Cities, 93, 120–135.

Firozjaei, M.K., Sedighi, A., Kiavarz, M., Qureshi, S., Haase, D., Alavipanah, S.K. (2019b). Automated Built-Up Extraction Index: A New Technique for Mapping Surface Built-Up Areas Using LANDSAT 8 OLI Imagery. Remote Sensing, 11, 1966.

Govil, H., Guha, H., Dey, A., Gil, A. (2019). Seasonal evaluation of downscaled land surface temperature: A case study in a humid tropical city, Heliyon, Volume 5, Issue 6, e01923, ISSN 2405-8440, https://doi.org/10.1016/j.heliyon.2019.e01923.

Granero-Belinchon, C., Michel, A., Lagouarde, J.-P., Sobrino, J.A., Briottet, X. (2019). Multi-Resolution Study of Thermal Unmixing Techniques over Madrid Urban Area: Case Study of TRISHNA Mission. Remote Sensing, 11, 1251.

Haashemi, S., Weng, Q., Darvishi, A., Alavipanah, S.K. (2016). Seasonal Variations of the Surface Urban Heat Island in a Semi-Arid City. Remote Sensing, 8, 352-856. https://doi.org/10.3390/rs8040352.

He, C., Shi, P., Xie, D., Zhao, Y. (2010). Improving the normalized difference built-up index to map urban built-up areas using a semiautomatic segmentation approach. Remote Sensing Letters., 1, 213–221.

Indian National SATellite Very High Resolution Radiometer (INSAT 3A), https://directory.eoportal.org/web/eoportal/satellite-missions/i/insat-3. (accessed on 10 December 2020)

Kohonen T, (2001). Self-Organizing Maps " 3rd edition, Springer, Berlin.

Kustas,W.P., Norman, J.M., Anderson, M.C., French, A.N. (2003). Estimating subpixel surface temperatures and energy fluxes from the vegetation index–radiometric temperature relationship. Remote Sensing of Environment, 85, 429–440.

Li, S., Mo, H., Dai, Y. (2011). Spatio-temporal pattern of Urban Cool Island Intensity and its eco-environmental response in Chang-Zhu-Tan Urban Agglomeration. Communications in information science and management engineering.

Mallick, J., Singh, C. K., Shashtri, S., Rahman, A., Mukherjee, S. (2012). Land surface emissivity retrieval based on moisture index from LANDSAT TM satellite data over heterogeneous surfaces of Delhi City. International Journal of Applied Earth Observation and Geoinformation, 19, 348 - 358

Mugiraneza, T., Ban, Y., Haas, J. (2019). Urban land cover dynamics and their impact on ecosystem services in Kigali, Rwanda using multi-temporal Landsat data. Remote Sensing Applications: Society and Environment 2019, 13: 234-246. https://doi.org/10.1016/j.rsase.2018.11.001

Ngo, K. D., Lechner, A. M., Vu, T. T. (2020). Land cover mapping of the Mekong Delta to support natural resource management with multi-temporal Sentinel-1A synthetic aperture radar imagery. Remote. Remote Sensing Applications: Society and Environment, Volume 17, 100272. https://doi.org/10.1016/j.rsase.2019.100272

Nichol, J. (1996). High-resolution surface temperature patterns related to urban morphology in a tropical city: A satellite-based study. Journal of applied meteorology, 35, 135–146.

Owen, T. W., Carlson, T. N., Gillies, R. R. (1998). An assessment of satellite remotely-sensed land cover parameters in quantitatively describing the climatic effect of urbanization, International Journal of Remote Sensing, 19:9, 1663-1681 To link to this article: http://dx.doi.org/10.1080/014311698215171

Pan, X., Zhu, X., Yang, Y. et al. (2018). Applicability of Downscaling Land Surface Temperature by Using Normalized Difference Sand Index. Scientific Reports 8, 9530. https://doi.org/10.1038/s41598-018-27905-0

PHG. Palestinian Hydrology Group for Water and Environmental Resources Development, Quality use of Home Reverse Osmosis Filters of Some Areas in Gaza Strip. (2002)

Rahman, M.T., Aldosary, A.S., Mortoja, M.G. (2017). Modeling future land cover changes and their effects on the land surface temperatures in the Saudi Arabian eastern coastal city of Dammam. Land, 6, 36, doi:10.3390/land6020036

Rasul, A., Balzter, H., Ibrahim, G.R.F., Hameed, H.M., Wheeler, J., Adamu, B., Ibrahim, S., Najmaddin, P.M. (2018). Applying Built-Up and Bare-Soil Indices from Landsat 8 to Cities in Dry Climates. Land, 7, 81. doi:10.3390/land7030081

Rasul, A., Balzter, H., Ibrahim, G.R.F., Hameed, H.M., Wheeler, J., Adamu, B., Ibrahim, S., Najmaddin, P.M. (2018). Applying Built-Up and Bare-Soil Indices from Landsat 8 to Cities in Dry Climates. Land, 7, 81. doi:10.3390/land7030081

Rasul, A., Balzter, H., Smith C. (2015). Spatial variation of the daytime Surface Urban Cool Island during the dry season in Erbil, Iraqi Kurdistan, from Landsat 8. Urban Climate, 14(2), 176-186, https://doi.org/10.1016/j.uclim.2015.09.001.

Rasul, A., Balzter, H., Smith, C. (2016). Diurnal and Seasonal Variation of Surface Urban Cool and Heat Islands in the Semi-Arid City of Erbil, Iraq. Climate, 4, 42.

Rasul, A., Balzter, H., Smith, C., Remedios, J., Adamu, B., Sobrino, J.A., Srivanit, M., Weng, Q. A. (2017). Review on Remote Sensing of Urban Heat and Cool Islands. Land, 6, 38. https://doi.org/10.3390/land6020038

Sobrino, J.A., Jiménez-Muñoz, J.C., Paolini, L. (2004). Land surface temperature retrieval from LANDSAT TM 5. Remote Sensing of Environment, 90, 434–440.

Sòria, G., Sobrino, J.A. (2007). ENVISAT/AATSR derived land surface temperature over a heterogeneous region. Remote Sensing of Environment, 111, 409–422.

Stathopoulou, M., Cartalis, C. (2009). Downscaling AVHRR land surface temperatures for improved surface urban heat island intensity estimation. Remote Sensing of Environment, 113, 2592–2605.

Sun, D., Pinker, R.T. (2003). Estimation of land surface temperature from a Geostationary Operational Environmental Satellite (GOES-8). Journal of Geophysical Research - Atmospheres, 108, doi:10.1029/2002JD002422.

Tan, K., Liao, Z., Du, P., Wu, L. (2016). Land surface temperature retrieval from Landsat 8 data and validation with geosensor network. Frontiers in Earth Science, doi:10.1007/s11707-016-0570-7.

Theeuwes, N., Steeneveld, G., Ronda, R., Rotach, M., Holtslag, A. (2015). Cool city mornings by urban heat. Environmental

Research Letters, 10, 11, http://dx.doi.org/10.1088/1748-9326/10/11/114022

Tucker, C.J., D'Souza, G., Belward, A.S., Malingreau, J.-P. (Eds.). (1996). Advances in the Use of NOAA AVHRR Data for Land Applications, Springer: Dordrecht, The Netherlands.

Voogt, J.A., Oke, T.R. (2003). Thermal remote sensing of urban climates. Remote Sensing of Environment, 86, 370–384.

Wang, K., Liang, S. (2009). Evaluation of ASTER and MODIS land surface temperature and emissivity products using long-term surface longwave radiation observations at SURFRAD sites. Remote Sensing of Environment, 113, 1556–1565.

Wicki, A., Parlow, E. (2017). Multiple Regression Analysis for Unmixing of Surface Temperature Data in an Urban Environment. Remote Sensing, 9, 684.

Yang, Y., Cao, C., Pan, X., Li, X., Zhu, X. (2017). Downscaling Land Surface Temperature in an Arid Area by Using Multiple Remote Sensing Indices with Random Forest Regression. Remote Sensing, 9, 789.

Zakšek, K., and K. Oštir. (2012). Downscaling Land Surface Temperature for Urban Heat Island Diurnal Cycle Analysis. Remote Sensing of Environment, 117: 114–124. doi:10.1016/j.rse.2011.05.027.

Zha, Y., Gao, J., Ni, S. (2003). Use of normalized difference built-up index in automatically mapping urban areas from TM imagery. International Journal of Remote Sensing, 24, 583–594.

Zhou, J., Chen, Y., Wang, J., Zhan, W. (2011). Maximum nighttime urban heat island (UHI) intensity simulation by integrating remotely sensed data and meteorological observations. IEEE Journal of Selected Topics in Applied Earth Observations and Remote Sensing, 4, 138–146.

Zhou, J., Zhang, X., Zhan, W., Zhang, H. (2014). Land surface temperature retrieval from MODIS data by integrating regression models and the genetic algorithm in an arid region. Remote Sensing, 6, 5344–5367.

Zhu, H., Guan, A. C. Millington, and G. Zhang. (2013). Disaggregation of land surface temperature over a heterogeneous urban and surrounding suburban area: a case study in Shanghai, China," International Journal of Remote Sensing, vol. 34, no. 5, pp. 1707–1723.